Influence of the electron distribution function shape on nonlocal electron heat transport in laser-heated plasmas

F. Alouani Bibi and J-P. Matte
INRS–Energie et Materiaux, Varennes, Quebec, Canada J3X 1S2

(Received 17 June 2002; revised manuscript received 22 August 2002; published 26 December 2002)

A nonlocal model of electron heat flow in laser-heated plasmas taking into account the super-Gaussian deformation of the electron velocity distribution function by the laser heating was developed. Based on comparisons to Fokker-Planck simulations of hot spot heating, it performs better than previous models. The growth rate of thermal filamentation is considerably changed by this thermal conductivity modification. First results from a formula describing the isotropic component, $f_0(x,v)$, of the electron velocity distribution function as a spatial convolution over local Maxwellians are also presented.

DOI: 10.1103/PhysRevE.66.066414 PACS number(s): 52.25.Fi, 52.38.Dx, 52.38.Hb, 52.65.Kj

In modeling plasma dynamics with hydrodynamic equations, classical Spitzer-Härm (SH) [1] thermal conductivity is used to obtain the electron heat flux from the local temperature gradient: $\vec{q}_e = -\kappa_{\mathrm{SH}} \vec{\nabla} T_e$. This formula breaks down if the temperature gradient is steep, and this sets in at a rather low value of λ/L, the ratio of the mean free path to the temperature scale length [2–9]. In laser-heated plasmas, such steep gradients often occur. Ad hoc flux limiting, i.e., limiting the classical heat flux to a fraction f of the free-streaming flux $[q_{\max} = f(k_B T_e)^{3/2}/\sqrt{m_e}]$ is an often-used device [10], but it is not satisfactory both because of the arbitrary value of f—usually, it is varied until agreement with experiment is obtained—and because it does not describe preheating at the foot of the heat front. A considerable improvement was brought by nonlocal heat-flow formulas, which consist of spatial convolutions over the classical Spitzer-Härm heat flux [4–9], and the large range of their kernel reflects the fact that heat flow is carried by high-energy electrons, whose mean free path is much longer than that of the bulk. However, there have been recent reports of unsatisfactory performance in simulating plasmas heated by intense laser beams. X-ray line ratio measurements during double short pulse experiments by Kieffer's group [11] could not be properly simulated with a hydrodynamic simulation using the Epperlein-Short [6] nonlocal heat-flow formula, but the line ratios could be reproduced either with an electron kinetic code or by assuming an arbitrary flux limit $f = 0.07$ in the hydrodynamic code simulation. More recently, Brunner and Valeo performed extensive electron kinetic simulations of multiple and single hot spot heating, in both planar and cylindrical geometry [12]. Comparing the temperature profiles computed in some of these with hydrodynamic simulations using one of these nonlocal heat-flow formulas, that of Bychenkov *et al.* [7–9], they found good agreement at low intensity, but a large discrepancy at high intensity [12]. Therefore, our chief objective here has been to develop an improved description of nonlocal electron heat flow in the presence of strong collisional heating. A second goal was to develop an analogous convolution formula (over local Maxwellians) to estimate the deformation of the distribution function by the combined effects: transport and heating. This is important because, even if we have a very accurate heat-flow algorithm and therefore correct temperature (defined as $\frac{2}{3}$ average energy) profiles, important properties of the plasma would still be incorrectly calculated: Non-Maxwellian distribution functions have important effects on ion (acoustic) and electron (Langmuir) plasma waves, and hence on Brillouin and Raman stimulated scattering instabilities [13], as well as on rates of ionization and excitation and x-ray spectra [14–16], hence the desirability of obtaining these without the very high computational cost of kinetic simulations. The measure of success for both goals is by comparison to electron kinetic simulations. A key aspect of the problem is the fact that, even in a uniform plasma, inverse bremsstrahlung (collisional) laser heating tends to create a super-Gaussian or ''DLM'' (Dum-Langdon-Matte) distribution function $f_m(v) = C_m \exp[-(v/v_m)^m]$ [15–18], where the index m is an increasing function [15,16] of the parameter $\alpha = Z(v_{\mathrm{osc}}/v_{\mathrm{th}})^2$, and $2 \leqslant m \leqslant 5$, with $m = 2$ corresponding to the Maxwellian weak heating limit and $m = 5$ to the strong heating limit when the heating is much more rapid than relaxation by electron-electron collisions [17]. Here, Z is the ion charge state, $v_{\mathrm{osc}} = |eE|/m_e\omega_0$ is the velocity of oscillation of the electrons in the laser field E, $v_{\mathrm{th}} = (k_B T_e/m_e)^{1/2}$ is the electron thermal velocity, and ω_0 is the laser angular frequency. Mora and Yahi have shown analytically that, for small gradients, such distributions lead to a strongly reduced thermal conductivity [19]. This aspect of the problem was not included in almost all previously published nonlocal heat-flow formulas [4–9].

Two numerical codes were used in the present work: (i) The hydrodynamic code HYDRO+, which solves the electron heat diffusion equation with either our nonlocal heat-flow formula, one of several previously published ones, or the more traditional flux limiter; and (ii) the electron kinetic code FPI [3,13–16,20], which was used both to develop our formula, and as a basis for comparison of heat-flow models. Briefly, FPI is one-dimensional (1D) (planar) in space and 2D in velocity space $(v, \mu = v_x/v)$, with a Legendre polynomial expansion for the μ dependence, which was carried to order 3 in this work. The included physical processes are advection (transport term, $v_x \partial F/\partial x$), a self-consistent space-charge field for quasineutrality and the resulting acceleration $[-(eE/m)\partial F/\partial v_x]$, Fokker-Planck terms for electron-ion

and electron-electron collisions, and heating by collisional absorption (inverse bremsstrahlung, or IB), using the kinetic heating operator described in Ref. [17]. To isolate transport phenomenology, the same laser intensity profile was imposed in both codes. The ions were either immobile or considered as a cold fluid. As an option, the ponderomotive pressure was included as a simple force term.

We now turn to the development of our nonlocal heat-flow formula. Usually the nonlocal heat flux is expressed as a convolution over the Spitzer-Härm flux with a nonlocal kernel. This form was first derived from the Fokker-Planck equation by Luciani and Mora [4] and was used later in all published nonlocal models [4–9]. We will therefore use this notation for the nonlocal heat flux, i.e.,

$$q(x)=\int_{-\infty}^{+\infty} w(\xi(x,x'))q_{\mathrm{SH}}(x')dx', \tag{1}$$

where q_{SH} is the Spitzer-Härm flux, w is the nonlocal propagator or kernel,

$$\xi(x,x')=\frac{1}{\lambda_e(x',Z)}\left|\int_{x'}^{x}\frac{N_e(x'')}{N_e(x')}dx''\right|,$$

$$\lambda_e(x',Z)=v_{\mathrm{th}}/\nu_{\mathrm{ei}} \tag{2}$$

λ_e is the electron mean free path, while ν_{ei} is the mean electron-ion collision frequency at velocity v_{th}.

To account for the ''DLM'' distribution's effect, we introduce an α dependence into the propagators. To evaluate these, we have run our electron kinetic code ''FPI'' in a perturbation mode following the method used by Epperlein and Short [21], whose work was the first to address the issue of nonlocal heat-flow modification due to this distribution function effect: an initially homogeneous plasma is heated by a uniform laser field with a small intensity modulation. In these runs, the ions are immobile and the ponderomotive force is not included. We varied the intensity of the laser field from one run to the next (but always imposing a 1% intensity modulation), which directly affected the heating time and the value of α. This procedure was done for a large number of values of Z and α, and, for each (α,Z), for many values of $k\lambda_e$. The ratio of the Fourier component of the FPI heat flux ($q\sim\int f_1 v^5 dv$) to the SH one (obtained from the FPI T_e modulation, where $T_e=\frac{2}{3}$ average energy) gave the Fourier transform of the heat-flow propagator for this particular wave vector, i.e.,

$$\tilde{w}(k\lambda_e,\alpha,Z)=\frac{\tilde{q}(k\lambda_e,\alpha,Z)}{\tilde{q}_{\mathrm{SH}}(k\lambda_e,Z)}\equiv\frac{\tilde{\kappa}(k\lambda_e,\alpha,Z)}{\tilde{\kappa}_{\mathrm{SH}}(k\lambda_e,Z)}. \tag{3}$$

For example, the results for plastic CH ($Z=5.3$) at several values of α are plotted in Fig. 1. It is seen that for long wavelengths, the conductivity is reduced for higher α, as noted in Ref. [19], but the opposite is true at short wavelength. To explain this behavior, we have examined the perturbed distribution functions in detail (not shown), and found that for a Maxwellian distribution function but high $k\lambda_e$, the traditional heat carrier electrons ($v\approx 3.7v_{\mathrm{th}}$) are decoupled

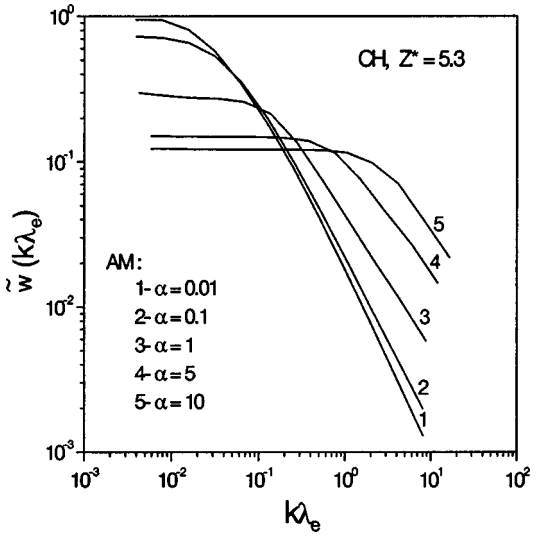

FIG. 1. Thermal conductivity correction obtained by our Fokker-Planck code for CH ($Z=5.3$), as a function of $k\lambda_e$ at different values of the Langdon parameter α [$\alpha=Z(v_{\mathrm{osc}}/v_{\mathrm{th}})^2$].

from the thermal bulk and then the real heat carriers are less energetic and hence more collisional and less effective to carry the heat flow. This is principally due to the fact that the mean free path of these $3.7v_{\mathrm{th}}$ electrons is longer than the perturbation wavelength, so that their spatial modulation is effectively reduced by transport effects for the case of low α. For the super-Gaussian case or at high α, even for long wavelengths, the heat-flow carriers ($v\approx 2.8v_{\mathrm{th}}$) already have shorter mean free path length and are then not decoupled from the thermal bulk of the electron velocity distribution function (EVDF), which means a more effective thermal conduction for a super-Gaussian than for a Maxwellian at short perturbation wavelengths, in addition to the fact that their spatial modulation is maintained by the modulation of the intensity. An additional increase of the propagator values is observed for all values of α as we move to higher Z, due to the increase of collisionality.

From the inverse Fourier transforms of these $\tilde{w}(k\lambda_e,\alpha,Z)$, we obtained the heat flux propagators. They are well fitted by the expression

$$w(\xi(x,x',Z),\alpha(x'),Z)=\frac{1}{\lambda_e(x',Z)}\left[\frac{a_1[\alpha(x')]}{(1+\{a_2[\alpha(x')]\xi(x,x',Z)\}^{a_3[\alpha(x')]})}\right], \tag{4}$$

where the parameters a_1, a_2, a_3 have a dependency on α that can be approximated as follows:

$$a_1(\alpha)=0.016\,913\,66\alpha^{0.317\,328\,56}+0.024\,025\,95,$$

$$a_2(\alpha)=0.596\,959\,85\alpha^{0.516\,534\,99}+0.096\,182\,82,$$

$$a_3(\alpha)=0.414\,361\,44\alpha^{0.345\,655\,93}+0.898\,267\,64.$$

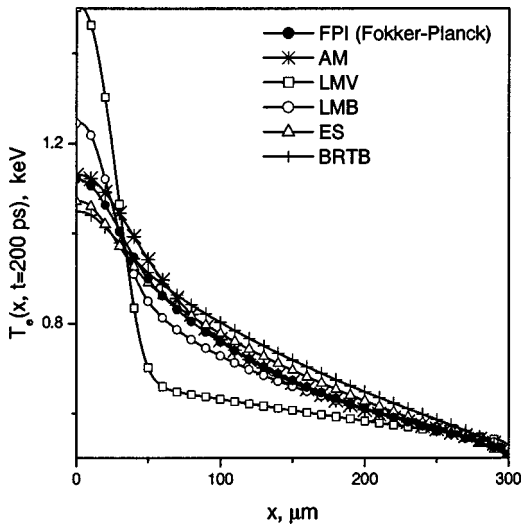

FIG. 2. Comparison of the temperature profiles in a laser-heated plasma (●) Fokker-Planck results (FPI), (*) our newly developed model (AM), and other published nonlocal models: (□) Luciani-Mora-Virmont [4], (○) Luciani-Mora-Bendib [5], (△) Epperlein-Short [6], and (+) Bychenkov-Rozmus-Tikhonchuk-Brantov [7]. $I_0=10^{15}$ W/cm^2, $Z=11$. FWHM (temporal) 200 ps and FWHM (spatial) 38 μm. The profiles are presented at the laser-pulse maximum (200 ps).

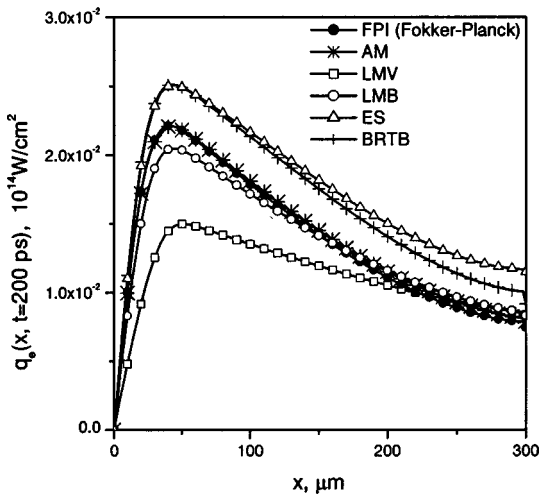

FIG. 3. Comparison of the heat-flux profiles in a laser-heated plasma (●) Fokker-Planck results (FPI), (*) our newly developed model (AM), and other published nonlocal models: (□) Luciani-Mora-Virmont [4], (○) Luciani-Mora-Bendib [5], (△) Epperlein-Short [6], and (+) Bychenkov-Rozmus-Tikhonchuk-Brantov [7]. $I_0=10^{15}$ W/cm^2, $Z=11$. FWHM (temporal) 200 ps and FWHM (spatial) 38 μm. The profiles are presented at the laser-pulse maximum (200 ps).

Note that α is evaluated at the source point, x', in Eq. (4): This is because the physics involved is the modification of the source for the heat flux, due to the non-Maxwellian electron distribution there. This formula was included in our HYDRO+ code to give the nonlocal heat flux. The reduction of the absorption calculated by Langdon as a function of α [17] is included in the code. Also, at high intensities, a further reduction of absorption occurs, due to the finite value of the ratio $v_{\rm osc}/v_{\rm th}$, and is accounted for by the correction factor obtained by Schlessinger and Wright [22]: $(1+v_{\rm osc}^2/v_{\rm th}^2)^{-3/2}$. A corresponding (velocity dependent) correction to the electron-ion collision rate is also included in the electron kinetic code FPI [20].

As a first application of this formula, we have used the case of an initially uniform underdense plasma ($n_e=2\times10^{20}$ cm^{-3}, $T_e=500$ eV) heated by a narrow [full width at half maximum (FWHM) equal to 38 μm] and intense laser beam ($I_0=10^{15}$ W/cm^2, $\lambda_0=0.53$ μm), as a test bed for the study of these nonlocal and non-Maxwellian effects. The geometry considered here is planar and transverse to the laser beam propagation, which means that the assumed narrow laser beam is line-focused, with a very long waist and negligible attenuation along its direction of propagation. The spatial variation is in the direction normal to the plane containing the propagation axis and to the (infinite) beam width. To isolate transport effects, the laser intensity profile was prescribed to be Gaussian in both time (FWHM equal to 200 psec) and space (FWHM equal to 38 μm), and, in the first runs, ions were kept immobile and the ponderomotive force was not included. This simulates the heating of a preformed plasma by a single hot spot, as studied in recent experiments by Montgomery *et al.* [23]. In Figs. 2 and 3, we compare the electron temperature and heat flux profiles at the peak of the pulse obtained with our electron kinetic code FPI with that obtained with our Eulerian hydrodynamic code HYDRO+ using our nonlocal heat-flow model (AM) and with other nonlocal heat-flow models of Luciani *et al.* (LMV [4], LMB [5]) and the more recent formulas of Epperlein and Short (ES [6]) and of Bychenkov *et al.* (BRTB [7–9]). We have presented in Figs. 2 and 3 just one-half of the temperature and heat flux profiles because of the symmetry of T_e and the antisymmetry of q_e with respect to $x=0$, which is due to the fact that the laser beam considered here is symmetric and centered at $x=0$. As can be seen, our model reproduces the temperature profiles as well as the heat fluxes obtained by the detailed kinetic calculation (FPI) ($T_e\sim\int f_0 v^4 dv$, $q_e\sim\int f_1 v^5 dv$) extremely well and noticeably better than the other nonlocal heat-flow models for the case considered here. The computation time was little more than that needed for hydrodynamic calculations with the traditional flux-limited heat-flow calculation, and very much less than the kinetic simulations. The temperature profiles obtained with flux limiters (not shown) were very different from the FPI one, for any value of the flux limit. We have done similar comparisons in cases with different Z and different laser parameters as well as cases with mobile ions (treated as a cold fluid in both codes) and with and without the ponderomotive force (included here as a simple force term), and again found excellent performance for our heat-flow model.

As a second application of our thermal conductivity formula, this time to ICF (inertial confinement fusion), we have used it to compute the spatial growth rate of laser filamentation in a laser-heated plasma. For this purpose we use the expression given in Ref. [6],

$$K=\frac{k_\perp}{2\sqrt{\varepsilon}}\left\{2\frac{n_e}{n_c}\left[\gamma_P+\gamma_T\left(\frac{\kappa_{\rm SH}}{\kappa}\right)\frac{\omega^2}{k_\perp^2c^2}\right]-\frac{k_\perp^2c^2}{\omega^2}\right\}, \qquad (5)$$

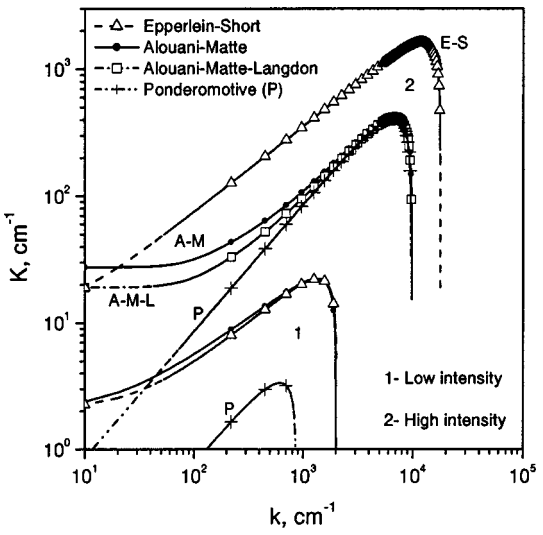

FIG. 4. Spatial growth rate K (cm^{-1}) as a function of the perturbation wave number k (cm^{-1}); (AM, ——) represents our model; (ES, – – –) the Epperlein-Short model; (P,———) the ponderomotive filamentation growth rate; (AML, – - – -) our model plus the reduction of γ_T due to the Langdon effect: 1, $I_0=10^{13}$ W/cm^2; $\lambda_0=1.06$ μm; $T_e=0.8$ keV; $n_e/n_c=0.1$; $Z=5.3$. 2, $I_0=2.5\times10^{15}$ W/cm^2; $\lambda_0=1.06$ μm; $T_e=2$ keV; $n_e/n_c=0.1$; $Z=20$.

where $k_\perp$ is the perturbation wave number perpendicular to the direction of propagation, c is the speed of light, ω is the laser frequency, $\varepsilon=1-n_e/n_c$, and the values of γ_P and γ_T are also defined and given in [6],

$$\gamma_P=\frac{(\text{ponderomotive pressure})}{(\text{plasma thermal pressure})},$$

$$\gamma_T=\frac{(\text{inverse bremsstrahlung heating rate})}{(\text{thermal conduction rate across}\, c/\omega)}$$

and the ratio $(\kappa/\kappa_{\mathrm{SH}})$ is that computed from Eq. (3) and plotted in Fig. 1 for our model (AM), and that taken from Ref. [6] for the curves labeled (ES).

The results are shown in Fig. 4. If we consider a low intensity situation, as in Ref. [6] (case 1: $I_0=10^{13}$ W/cm^2, $\lambda_0=1.06$ μm, $T_e=0.8$ keV, $n_e/n_c=0.1$, $Z=5.3$), then we (AM) get nearly the same results as theirs (ES), the validity of which was confirmed by the comparison with Young's low-intensity experiments [24]. This is so because, in this case, the electron distribution function is nearly Maxwellian due to the low value of α. We also show the effect of ponderomotive (P) filamentation alone, obtained by setting $\gamma_T=0$ in Eq. (5), and it is easily seen that thermal effects are dominant at low intensity. However, higher intensities are more relevant to ICF. We have considered a case in which α is about 11.07 (case 2: $I_0=2.5\times10^{15}$ W/cm^2, $\lambda_0=1.06$ μm, $T_e=2$ keV, $n_e/n_c=0.1$, $Z=20$). According to the Epperlein model (ES), there would be a large enhancement of the growth rate over the ponderomotive one (P) by thermal effects at all wave vectors, whereas our heat-flow model (AM) indicates such an enhancement only at low wave vectors, but none at higher ones. This is due to the fact that the heat conductivity reduction at high k is far less when α is high (see Fig. 1), so that thermal conductivity can suppress thermal filamentation in this case. A further reduction of the thermal effects is due to the reduction in absorption when α is this high: Langdon's formula [17] indicates that absorption is then reduced by $R(\alpha)=0.49$. The curve AML reflects this [γ_T was reduced accordingly in Eq. (5)]. While noticeable, this effect is less important than the differences between the thermal conductivity models.

As motioned earlier, in the laser intensity ranges of the ICF experiments (10^{15}–10^{16} W/cm^2) the EVDF (electron velocity distribution function) almost always has a non-Maxwellian form in the underdense plasma. In the overdense plasma, there is a surplus of fast electrons due to nonlocal transport. This can affect other plasma characteristics than the thermal conductivity or particle transport: atomic physics (ionization and excitation reaction rates) [15], acoustic and Langmuir wave propagation [13], and absorption [17]. Thus, having a correct temperature profile is not sufficient. A knowledge of the electron distribution function is required to describe these processes. Toward this end, we have adopted the same approach as for the nonlocal heat flux, i.e., we performed a series of FPI runs for initially homogeneous plasmas heated by a uniform laser field with a small intensity modulation. A kernel expression analogous to the one developed for the heat flux [Eq. (3)] was obtained as a ratio of the Fourier transforms of the calculated EVDF (f_0) and the local Maxwellian distribution, i.e.,

$$\tilde{g}(k,\alpha,v)=\tilde{f}_0(k,\alpha,v)/\tilde{f}_M(k,v). \tag{6}$$

This implies that

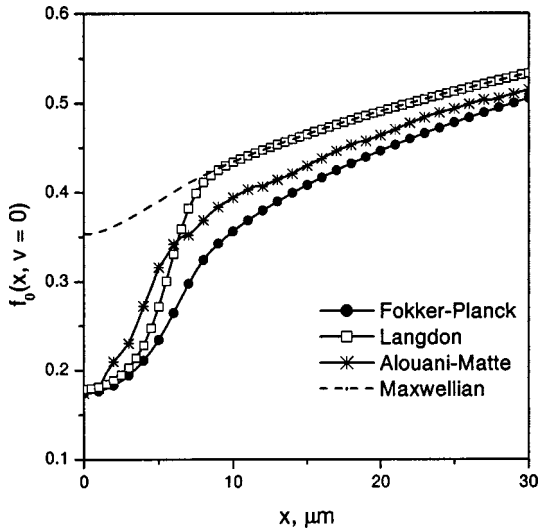

FIG. 5. Isotropic component of the electron EVDF for $v=0$; $I_0=1\times10^{15}$ W/cm^2, $\lambda_0=0.53$ μm, FWHM (temporal)=200 ps, FWHM (spatial)=38 μm, $Z=11$. (—●—) Fokker-Planck solution (FPI), (– – –) the local Maxwellian distribution, (—*—) our newly developed model for the EVDF, (—□—) the Langdon function.

$$f_0(x,v)=\int_{-\infty}^{+\infty} g(\xi(x,x'),\alpha(x'),v) f_M(x',v)\,dx'. \quad (7)$$

Comparisons between the EVDF at zero velocity calculated by Eq. (7), the numerical solution of the Fokker-Planck Equation (FPI), the local Maxwellian, and the Langdon correction to it [17] were made. The value at zero velocity is particularly important as it determines absorption. An example of the obtained results is illustrated in (Fig. 5), for $I_0=10^{15}$ W/cm^2, $\lambda_0=0.53$ μm, FWHM equal to 200 psec, and 38 μm, $n_e/n_c=0.2$, $Z=11$. We can see in this example that although this model is rather simple and uses a convolution over local Maxwellians, the results obtained can be considered as a satisfactory approximation to the numerical solution of the Fokker-Planck equation.

In conclusion, we can note that nonlocal effects in plasmas in general, and in laser-created plasma in particular, are strongly related to the form of the electron distribution function created by the heating mechanism. We have considered this aspect here, and the results of our nonlocal model showed a good agreement for the temperature profiles with the Fokker-Planck simulation results. Also, this model has shown important changes in the growth rate of one of the important parametric instabilities for ICF, filamentation. This approach to computing the isotropic part of the EVDF is very promising as it will make it possible to reproduce the numerical Fokker-Planck solution by using a set of local Maxwellians, which can be useful in hydrodynamic codes for the modeling of several kinetic effects.

We thank Dr. D.S. Montgomery, Dr. V.Yu. Bychenkov, Dr. B.B. Afayan, Dr. E.A. Williams, Dr. R.L. Berger, Dr. A. Maximov, Dr. G.P. Schurtz, Professor J.C. Kieffer, and Dr. F. Vidal for useful discussions. This research was partially supported by the Ministère de l'Éducation du Québec and by the Natural Sciences and Engineering Council of Canada.

[1] L. Spitzer and R. Härm, Phys. Rev. **89**, 977 (1953).
[2] A. R. Bell, R. Evans, and D. J. Nicholas, Phys. Rev. Lett. **46**, 243 (1981).
[3] J. P. Matte and J. Virmont, Phys. Rev. Lett. **49**, 1936 (1982).
[4] J. F. Luciani, P. Mora, and J. Virmont, Phys. Rev. Lett. **51**, 1664 (1983).
[5] J. F. Luciani, P. Mora, and A. Bendib, Phys. Rev. Lett. **55**, 2421 (1985).
[6] E. M. Epperlein and R. W. Short, Phys. Fluids B **4**, 2211 (1992); Phys. Rev. Lett. **65**, 2145 (1990).
[7] V. Bychenkov *et al.*, Phys. Rev. Lett. **75**, 4405 (1995).
[8] A. V. Brantov *et al.*, JETP **83**, 716 (1996).
[9] V. Bychenkov *et al.*, Phys. Plasmas **5**, 2742 (1998).
[10] R. C. Malone, R. L. McCrory, and R. L. Morse, Phys. Rev. Lett. **34**, 721 (1975).
[11] C. Y. Côté, J. C. Kieffer, and O. Peyrusse, Phys. Rev. E **56**, 992 (1997).
[12] S. Brunner and E. Valeo, Phys. Plasmas **9**, 923 (2002).
[13] B. B. Afeyan *et al.*, Phys. Rev. Lett. **80**, 2322 (1998).
[14] J. P. Matte *et al.*, Phys. Rev. Lett. **72**, 1208 (1994).
[15] P. Alaterre, J. P. Matte, and M. Lamoureux, Phys. Rev. A **34**, 1578 (1986).
[16] J. P. Matte *et al.*, Plasma Phys. Controlled Fusion **30**, 1665 (1988).
[17] A. B. Langdon, Phys. Rev. Lett. **44**, 575 (1980).
[18] C. T. Dum, Phys. Fluids **21**, 945 (1978); **21**, 956 (1978).
[19] P. Mora and H. Yahi, Phys. Rev. A **26**, 2259 (1982).
[20] S. Ethier and J. P. Matte, Phys. Plasmas **8**, 1650 (2001), and references therein.
[21] E. M. Epperlein and R. W. Short, Phys. Rev. E **50**, 1697 (1994).
[22] L. Schlessinger and J. Wright, Phys. Rev. A **20**, 1934 (1979).
[23] D. S. Montgomery *et al.*, Phys. Plasmas **3**, 1728 (1996).
[24] P. E. Young, Phys. Plasmas **2**, 2815 (1995).